Cluster structures and monopole transitions of ^{14}C

Yoshiko Kanada-En'yo[1] and Kazuyuki Ogata[2,3,4]
[1]*Department of Physics, Kyoto University, Kyoto 606-8502, Japan*
[2]*Research Center for Nuclear Physics (RCNP), Osaka University, Ibaraki 567-0047, Japan*
[3]*Department of Physics, Osaka City University, Osaka 558-8585, Japan*
[4]*Nambu Yoichiro Institute of Theoretical and Experimental Physics (NITEP), Osaka City University, Osaka 558-8585, Japan*

(Received 22 September 2019; revised manuscript received 17 November 2019; published 22 January 2020)

Cluster structures of ^{14}C were investigated with a method of antisymmetrized molecular dynamics (AMD) combined with a $3\alpha + nn$ cluster model while focusing on the monopole excitations and the linear-chain 3α band. Variation after parity and angular-momentum projections was performed in the AMD framework, and the generator coordinate method was applied to take into account various $3\alpha + nn$ cluster configurations. Energy spectra and monopole and $E2$ transition strengths of 0^+, 2^+, and 4^+ states were calculated to assign band structures. The 0^+_3 state with remarkable monopole transitions was obtained as a vibrational mode of the triangle 3α configuration. In addition, the linear-chain 3α band from the bandhead 0^+_4 state was obtained. ^{10}Be $+\alpha$ decay widths of 0^+, 2^+, and 4^+ states were evaluated. α inelastic scattering off ^{14}C was also investigated by the microscopic coupled-channel calculation with the g-matrix folding model to propose possible observation of the 0^+_3 state via α scattering experiments.

DOI: 10.1103/PhysRevC.101.014317

I. INTRODUCTION

3α clustering is one of the hot subjects of C isotopes. A variety of 3α cluster structures in ^{12}C have been investigated (see, for example, review articles [1–6] and references therein). Particularly, the 0^+_2 state of ^{12}C has been attracting a great interest and discussed as a gas state of α particles. The strong monopole transition from the ground state supports the developed 3α structure of the 0^+_2 state. In higher energies than the 0^+_2 state, other kinds of 3α-cluster structures such as a triangle, bending-chain, and higher-nodal states have been theoretically suggested [7–29].

For neutron-rich C isotopes, further rich phenomena of the 3α clustering are expected to appear because of surrounding excess neutrons. One of the fascinating topics is the linear-chain 3α structure in neutron-rich C. The linear-chain 3α clustering in ^{12}C was originally proposed by Morinaga [30,31], but it is considered to be unstable against bending motions. However, in the case of neutron-rich C isotopes, the linear-chain clustering can be stabilized owing to excess neutrons, as predicted in theoretical works [32–40]. In this decade, many experiments have been performed to observe cluster states in ^{14}C [41–48]. One of the good tools to search for new cluster states is α resonant scattering, which has been recently utilized to study cluster states in such unstable nuclei as ^{14}C. For ^{14}C, candidate states of the linear-chain band have been reported by recent experiments of the ^{10}Be $+\alpha$ resonant scattering [45–47], but its rotational band members have yet to be confirmed.

An alternative tool to investigate cluster states is the α inelastic scattering off target nuclei because developed cluster states tend to be populated by the α scattering via isoscalar transitions [49–56]. The α scattering has been utilized, in particular, to investigate isoscalar monopole transitions into excited 0^+ states as done for ^{16}O to study 0^+ cluster states [54].

Our aim is to investigate cluster states in ^{14}C focusing on the monopole excitations as well as α-decay property. In preceding works on the linear-chain structure of ^{14}C [34,37,40], methods of antisymmetrized molecular dynamics (AMD) [57–59] were applied, but the framework is not sufficient to describe detailed ^{10}Be $+\alpha$ clustering features. The cluster structures of ^{14}C have been also studied by the generator coordinate method (GCM) of a $3\alpha + nn$ cluster model [39]. However, the cluster model is not able to properly describe low-energy spectra because it is not suitable to describe shell-model configurations nor cluster breaking in low-lowing states. One of the authors [60] has studied low-lying states of ^{14}C by a calculation of variation after angular-momentum and parity projections (VAP) with the AMD model. The AMD calculation of VAP reasonably described the 0^+, 2^+, and 1^+ spectra and Gamow-Teller transitions from ^{14}N(1^+_1) except for the anomalously hindered β decay of the ground state of ^{14}C.

In the present paper, we apply the AMD method of VAP, combining it with the GCM of the $3\alpha + nn$ cluster model, which we call "VAP+cl-GCM" in this paper, and discuss the energy spectra and band structure of ^{14}C. Particular attention is paid to the monopole excitations and linear-chain band. Cluster features of ^{10}Be $+\alpha$ and $3\alpha + nn$ clusterings are discussed. The α inelastic scattering off ^{14}C are also calculated with the microscopic coupled-channel (MCC) calculation by using the matter and transition densities obtained by VAP+cl-GCM. The reaction approach is the g-matrix folding model, where α-nucleus coupled-channel potentials are microscop-

ically derived by folding the Melbourne g-matrix effective nuclear interaction with input of densities of the target nucleus from the structure model. Similar MCC calculations have been done for study of ^{12}C(α,α') and ^{16}C(α,α'), and proved to reproduce cross sections of cluster states without phenomenologically adjusting parameters of the reaction calculation [61–63].

The paper is organized as follows: The procedure of the structure calculation of VAP+cl-GCM is explained in Sec. II, and structure properties of ^{14}C are discussed in Sec. III. The result of the α scattering off ^{14}C is shown in Sec. IV. Finally, a summary is given in Sec. V.

II. FORMULATION OF VAP+CL-GCM

A. Model wave function

0^+ and 2^+ states of ^{14}C are calculated with the VAP version of AMD combined with the cluster GCM, in which AMD and $3\alpha + nn$ wave functions are superposed.

An AMD wave function is given by a Slater determinant of single-nucleon Gaussian wave functions as

$$\Phi_{\rm AMD}(\boldsymbol{Z}) = \frac{1}{\sqrt{A!}}\mathcal{A}\{\varphi_1,\varphi_2,\ldots,\varphi_A\}, \tag{1}$$

$$\varphi_i = \phi_{\boldsymbol{X}_i}\chi_i\tau_i, \tag{2}$$

$$\phi_{\boldsymbol{X}_i}(\boldsymbol{r}_j) = \left(\frac{2\nu}{\pi}\right)^{3/4}\exp[-\nu(\boldsymbol{r}_j-\boldsymbol{X}_i)^2], \tag{3}$$

$$\chi_i = \left(\frac{1}{2}+\xi_i\right)\chi_\uparrow + \left(\frac{1}{2}-\xi_i\right)\chi_\downarrow. \tag{4}$$

Here $\mathcal{A}$ is the antisymmetrizer, and φ_i is the ith single-particle wave function written by a product of spatial ($\phi_{\boldsymbol{X}_i}$), spin (χ_i), and isospin (τ_i fixed to be proton or neutron) wave functions. The width parameter ν is chosen to be the same value $\nu = 0.19$ fm^{-2} as in Ref. [60]. The parameters $\boldsymbol{Z} \equiv \{\boldsymbol{X}_1,\ldots,\boldsymbol{X}_A,\xi_1,\ldots,\xi_A\}$ for Gaussian centroid positions and nucleon-spin orientations of all nucleons are treated as variational parameters, which are optimized of each state of ^{14}C. We use five AMD wave functions ($\Phi^{(n)}_{\rm AMD}$ $n = 1,\ldots,5$) obtained for five states, ^{14}C$(0^+_{1,2}, 2^+_{1,2}, 1^+_1)$, with the energy variation after J^π (angular momentum and parity) projection in Ref. [60]. For more details, the reader is referred to this reference.

In addition to the AMD wave functions, $3\alpha + nn$ cluster wave functions are superposed to take into account large-amplitude motion between α clusters. The model wave functions for $3\alpha + nn$ configurations are almost same as those adopted in Ref. [39]. We first compose wave functions of the subsystem ^{10}Be with a $2\alpha + nn$ cluster model considering the α-α motion in ^{10}Be, and then place the third α cluster at various distances and angles from the ^{10}Be core, as illustrated by the schematic figure shown in Fig. 1. The first and second α clusters are placed on the Z axis at $(0,0,\pm d/2)$ with the distance d. For two valence neutrons, we adopt neutron configurations of a cluster model for ^{10}Be, as proposed by Itagaki *et al.* [64], which is an extended version of the Brink-Bloch cluster model [65]. Namely, wave functions for spin-up and -down neutrons are given by Gaussian wave packets at the same position but with the momentum opposite to each other. As a result, the $2\alpha + nn$ wave function is given as

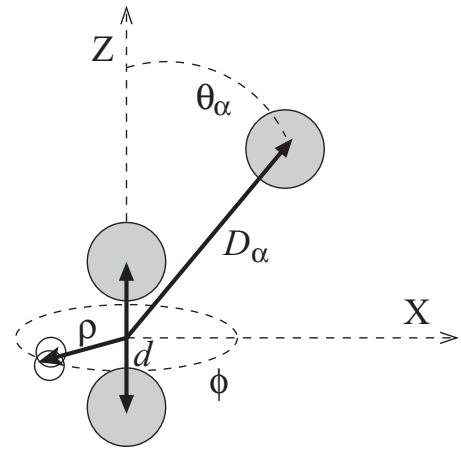

FIG. 1. Schematic figure of $(2\alpha + nn) + \alpha$ configurations used in the GCM basis wave functions of ^{14}C.

$$\Phi_{2\alpha+nn}(d,\phi) = \mathcal{A}[\Phi_\alpha(\boldsymbol{R}_1)\Phi_\alpha(\boldsymbol{R}_2)\varphi_{n\uparrow}(\boldsymbol{R}_{n\uparrow})\varphi_{n\downarrow}(\boldsymbol{R}_{n\downarrow})], \tag{5}$$

$$\varphi_{n\uparrow(\downarrow)}(\boldsymbol{R}_{n\uparrow(\downarrow)}) = \phi_{\boldsymbol{R}_{n\uparrow(\downarrow)}}\chi_{\uparrow(\downarrow)}, \tag{6}$$

with $\boldsymbol{R}_1 = -\boldsymbol{R}_2 = (0,0,d/2)$ and

$$\begin{aligned}\boldsymbol{R}_{n\uparrow} &= \rho(\cos\phi,\ \sin\phi,\ 0) + i\rho\Lambda(-\sin\phi,\ \cos\phi,\ 0),\\ \boldsymbol{R}_{n\downarrow} &= \rho(\cos\phi,\ \sin\phi,\ 0) - i\rho\Lambda(-\sin\phi,\ \cos\phi,\ 0).\end{aligned} \tag{7}$$

Here $\Phi_\alpha(\boldsymbol{R}_k)$ is the α cluster wave function given by the $(0s)^4$ harmonic-oscillator configuration located at $\boldsymbol{R}_k$ and the parameters ρ and Λ are optimized to minimize the ^{10}Be energy for each α-α distance d. Using the optimized values of ρ and Λ, the $3\alpha + nn$ wave function is given as

$$\begin{aligned}&\Phi_{3\alpha+nn}(d,D_\alpha,\phi,\theta_\alpha)\\ &\quad= \mathcal{A}[\Phi_\alpha(\boldsymbol{R}_1)\Phi_\alpha(\boldsymbol{R}_2)\Phi_\alpha(\boldsymbol{R}_3)\varphi_{n\uparrow}(\boldsymbol{R}_{n\uparrow})\varphi_{n\downarrow}(\boldsymbol{R}_{n\downarrow})],\end{aligned} \tag{8}$$

$$\boldsymbol{R}_3 = (D_\alpha\cos\theta_\alpha, 0, D_\alpha\sin\theta_\alpha). \tag{9}$$

To exactly remove the center-of-mass motion from the total wave function, the Gaussian center positions are shifted as $\boldsymbol{R}_k \to \boldsymbol{R}_k - \boldsymbol{R}_G$ and $\boldsymbol{R}_{n\uparrow(\downarrow)} \to \boldsymbol{R}_{n\uparrow(\downarrow)} - \boldsymbol{R}_G$ with $\boldsymbol{R}_G \equiv (4\sum_k \boldsymbol{R}_k + \boldsymbol{R}_{n\uparrow} + \boldsymbol{R}_{n\downarrow})/14$. The Gaussian widths of the α and neutron wave functions are common and taken to be the same ν value as that used in the AMD wave function. Note that the present $3\alpha + nn$ cluster wave function can be expressed by a specific configuration of the AMD wave function.

The basis wave functions $\Phi_{3\alpha+nn}(d,D_\alpha,\phi,\theta_\alpha)$ with various values of four parameters, d, D_α, ϕ, and θ_α, are projected to J^π eigenstates and superposed in the GCM calculation. We here simply denote the mth basis wave function as $\Phi^{(m)}_{3\alpha+nn}$ with the label m for the parameter set $(d,D_\alpha,\phi,\theta_\alpha)$. The final wave function of VAP+cl-GCM for the J^π_k state is obtained

by combining the AMD and the $3\alpha + nn$ wave functions as

$$\Psi(J_k^\pi) = \sum_{n,K} c_K^{(n)}(J_k^\pi) P_{MK}^{J\pi} \Phi_{\rm AMD}^{(n)} + \sum_{m,K} c_K^{\prime(m)}(J_k^\pi) P_{MK}^{J\pi} \Phi_{3\alpha+nn}^{(m)}, \quad (10)$$

where coefficients $c_K^{(n)}(J_k^\pi)$ and $c_K^{\prime(m)}(J_k^\pi)$ are determined by diagonalization of the norm and Hamiltonian matrices.

To evaluate component of a specific $3\alpha + nn$ configuration contained in the J_k^π state, we define the squared overlap of $\Psi(J_k^\pi)$ with a basis $3\alpha + nn$ wave function as

$$\mathcal{O}^2_{3\alpha+nn}(d, D_\alpha, \phi, \theta_\alpha) = \left|\left\langle \Psi(J_k^\pi) \middle| P_{MK}^{J\pi} \Phi_{3\alpha+nn}(d, D_\alpha, \phi, \theta_\alpha)\right\rangle\right|^2. \quad (11)$$

B. Effective interactions and parameter setting

We use the effective nuclear interactions of the MV1 (case 3) central force [66] supplemented by the spin-orbit term of the G3RS force [67,68], and the Coulomb force. The Bartlett, Heisenberg, and Majorana parameters, $b = h = 0.125$ and $m = 0.62$, in the MV1 force are adopted, and the strengths $u_I = -u_{II} = 3000$ MeV of the G3RS spin-orbit force are used. These interaction parameters are consistent with those used in Ref. [60] for the study of ^{14}C with the VAP calculation [60]. It should be commented that we use the MV1 force consisting of the finite-range two-body and zero-range three-body forces instead of the Volkoff force [69] used in Refs. [34,39], because spectra of low-lying states in ^{14}C and also those of cluster states in ^{16}O were reasonably reproduced by the MV1 force but not by the Volkoff force.

For the generator coordinates d, D_α, ϕ, and θ_α of the GCM calculation, we adopt discrete values, $d = 2, 3, 4$ fm, $D_\alpha = 2, 3, \ldots, 7$ fm, $\phi = \pi/8,\ 3\pi/8,\ 5\pi/8,\ 7\pi/8$, and $\theta_\alpha = 0,\ \pi/8,\ \pi/4,\ 3\pi/8,\ \pi/2$ of the $3\alpha + nn$ wave functions. Note that the angle ranges $0 \leqslant \phi \leqslant \pi$ and $0 \leqslant \theta_\alpha \leqslant \pi/2$ are equivalent to the full ranges $0 \leqslant \phi \leqslant 2\pi$ and $0 \leqslant \theta_\alpha \leqslant \pi$ because of the parity and angular-momentum projections. Note that, for configurations at $\theta_\alpha = 0$, the values $\phi = \pi/8,\ 3\pi/8,\ 5\pi/8,\ 7\pi/8$ are redundant because those wave functions are equivalent after angular-momentum projection due to the axial symmetry of the 3α part, and therefore only one of them is used. After reducing configurations for this redundancy, the number of basis $3\alpha + nn$ wave functions $\Phi_{3\alpha+nn}^{(m)}$ $(m = 1, \ldots, m_{\rm max})$ is $m_{\rm max} = (3 \times 4 \times 4 + 3) \times 6 = 306$.

The values of ρ and Λ of neutron wave functions are listed in Table I. In the first choice (set 1), we optimize ρ and Λ to minimize the 0^+ energy of the subsystem $P_{00}^{0+}\Phi_{2\alpha+nn}$. In the second choice (set 2), we use alternative values of ρ and Λ for $d = 3$ fm determined to minimize the $(J^\pi, K) = (2^+, 2)$ energy of $P_{M2}^{2+}\Phi_{2\alpha+nn}$ so as to globally optimize energies of ^{10}Be(0_1^+), ^{10}Be(2_1^+), and ^{10}Be(2_2^+). As shown in Table I, the second choice gives a better result of the low-energy energy spectra of ^{10}Be, in particular, the energy of ^{10}Be(2_2^+). Therefore, we adopt parameters ρ and Λ of set 2 in the present calculation of ^{14}C.

TABLE I. Optimized values of the ρ and Λ parameters and excitation energies of ^{10}Be of the first (set 1) and second (set 2) of $2\alpha + nn$ wave functions.

	ρ (fm), Λ		
	Set 1	Set 2	
$d = 2$ fm	(0.9,0.56)	(0.9,0.56)	
$d = 3$ fm	(1.5,0.38)	(1.9,0.02)	
$d = 4$ fm	(2.1,0.24)	(2.1,0.24)	
	E_x (MeV)		
	Set(1)	Set(2)	Expt.
^{10}B(2_1^+)	2.57	2.52	3.368
^{10}B(2_2^+)	7.64	6.38	5.958

III. STRUCTURE OF ^{14}C

A. Structure properties

The energy levels of ^{14}C obtained by the VAP+cl-GCM calculation are shown in Fig. 2. Root-mean-square radii and monopole transition strengths of the proton and neutron parts for 0^+ states are listed in Table II, and quadrupole ($\lambda = 2$) transition strengths of the proton and neutron parts are shown in Table III.

The calculated energy spectra of 0^+, 2^+, and 4^+ states are compared with the experimental energy spectra in Fig. 2. In the figure, the experimental levels with asterisk symbols are candidate states of the linear-chain band reported by the recent experiment of Ref. [47]. The 0_1^+ and 0_2^+ states are approximately described by the VAP wave functions showing shell-model like structure but no prominent cluster structure. In the mean-field picture, the 0_2^+ state is approximately understood as neutron excitation into a $(sd)^2$ configuration and has a normal proton radius as small as that of the ground state. In contrast to the 0_2^+ state, the 0_3^+ and 0_4^+ states have relatively large nuclear radii and spatially developed cluster structures. The 0_4^+ state dominantly has the linear-chain 3α structure and constructs a rotational band.

In the monopole transition strengths listed in Table II, the remarkable strength from the ground state is obtained for the

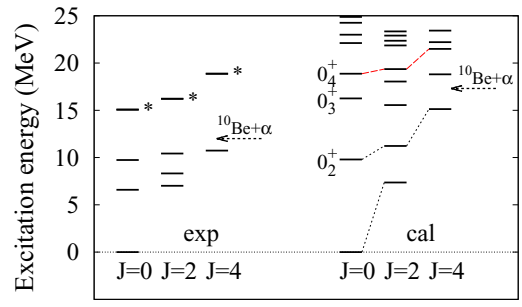

FIG. 2. The calculated energy spectra of 0^+, 2^+, and 4^+ states of ^{14}C are shown together with the experimental energy spectra assigned to 0^+, 2^+, and 4^+ in Ref. [70]. The experimental levels with asterisk symbols are the states reported in Ref. [47] as candidates of the linear-chain band.

TABLE II. Root-mean-square radii of $^{14}C(0_k^+)$ and monopole transition strengths from the ground state calculated with VAP+cl-GCM. Proton and neutron parts of radii (R_p and R_n) and monopole transition strengths [$B_p(E0)$ and $B_n(E0)$] are listed. The experimental proton radius of the ground state reduced from the experimental charge radius [71] is $R_p = 2.37$ fm.

	R_p (fm)	R_n (fm)	$B_p(E0)$ (fm^4)	$B_n(E0)$ (fm^4)
0_1^+	2.52	2.65		
0_2^+	2.62	2.80	1.1	2.5
0_3^+	2.98	2.98	18	15
0_4^+	3.48	3.37	1.0	0.7

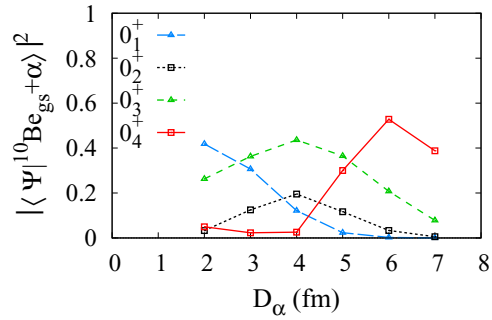

FIG. 3. The squared overlap of $\Psi(J_k^\pi)$ for the $0_{1,2,3,4}^+$ states with the $^{10}\mathrm{Be}(0_1^+) + \alpha$ wave function at the distance D_α.

0_3^+ state because of its nature of the triangle 3α vibration mode. On the other hand, the 0_4^+ state has weak monopole transition strength even though it is a developed cluster state, because the linear-chain state has the linearly aligned 3α configuration, which is much different from the ground state and difficult to be directly excited by the monopole operator.

Let us discuss the band structure based on the $E2$ transition strengths shown in Table III. The 2_1^+ state is assigned to the ground band and mainly contributed by the proton rotation. The 0_2^+, 2_2^+, and 4_1^+ states with dominant neutron $(sd)^2$ components construct the $K^\pi = 0_2^+$ band. The 0_3^+ state shows no clear signal of band structure. Instead, the $E2$ strength from this state is fragmented into 2_4^+ and 2_5^+ states. The rotational band of the linear-chain structure is built on the 0_4^+ state with the 2_5^+ and 4_3^+ states. This band shows a large moment of inertia (small level spacing) in the energy spectra and has remarkably strong $E2$ transitions due to the highly elongated structure: $B(E2: 2_5^+ \to 0_4^+) = 162$ (fm^4) and $B(E2: 4_3^+ \to 2_5^+) = 209$ (fm^4). More detailed properties of α decays and cluster structures are discussed in the following sections.

TABLE III. $E2$ transition strengths of $2^+ \to 0^+$ in ^{14}C calculated with VAP+GCM. In addition to the proton contribution $B(E2)$, the neutron contribution $[B_n(E2)]$ of the $\lambda = 2$ transitions is also shown. The strengths for $0_1^+ \to 2_{1,2,3,4,5}^+$ and those with $B(E2) \geqslant 2$ fm^4 or $B_n(E2) \geqslant 2$ fm^4 in the transitions $2_{1,2,3,4,5}^+ \to 0_{1,2,3,4}^+$ are given. The experimental value of $B(E2; 2_1^+ \to 0_1^+)$ is 3.6 ± 0.6 fm^4 [70].

	$B(E2)$ (fm^4)	$B_n(E2)$ (fm^4)
$2_1^+ \to 0_1^+$	7.8	2.4
$2_2^+ \to 0_1^+$	0.0	1.5
$2_3^+ \to 0_1^+$	0.1	0.0
$2_4^+ \to 0_1^+$	0.0	0.0
$2_5^+ \to 0_1^+$	0.1	0.1
$2_1^+ \to 0_2^+$	0.6	2.7
$2_2^+ \to 0_2^+$	6.8	43.2
$2_3^+ \to 0_2^+$	3.8	3.7
$2_4^+ \to 0_1^+$	3.3	0.7
$2_4^+ \to 0_3^+$	6.0	2.3
$2_5^+ \to 0_3^+$	29.0	33.5
$2_5^+ \to 0_4^+$	162	175

B. $^{10}\mathrm{Be}(0_1^+) + \alpha$ decay widths

To discuss α decay properties, we calculate the $^{10}\mathrm{Be}(0_1^+) + \alpha$ component in the 0^+, 2^+, and 4^+ states. The squared overlap of $\Psi(J_k^\pi)$ obtained by VAP+cl-GCM with the $^{10}\mathrm{Be}(0_1^+) + \alpha$ wave function with the distance D_α is calculated. The result for the $0_{1,2,3,4}^+$ states is shown in Fig. 3. The ground state has the overlap only in the internal region indicating the $^{10}\mathrm{Be}(0_1^+) + \alpha$ component as the ground-state correlation but no spatially developed clustering. In the 0_2^+ state, $^{10}\mathrm{Be}(0_1^+) + \alpha$ component is relatively minor compared with the 0_3^+ and 0_4^+ states. In the 0_3^+ state, the squared overlap is distributed in a wide range of D_α with the maximum amplitude at $D_\alpha = 4$ fm meaning that the α cluster is moving in the broad region around the $^{10}\mathrm{Be}(0_1^+)$ core. The 0_4^+ state has large overlap amplitudes at $D_\alpha = 6$ fm and shows remarkable development of the clustering. The significant amplitude at $D_\alpha = 7$ fm may indicate some coupling with $^{10}\mathrm{Be}(0_1^+) + \alpha$ continuum states.

We evaluate the reduced widths for $^{10}\mathrm{Be}(0_1^+) + \alpha$ from the calculated overlap with the approximation proposed in Ref. [72]. The energy spectra and widths for the states having significant decay widths are shown in Fig. 4. The energy levels are plotted with respect to relative energies (α-decay energies) E_r measured from the $^{10}\mathrm{Be} + \alpha$ threshold energy. Here, the partially decay widths for the $^{10}\mathrm{Be} + \alpha$ channel are evaluated with the reduced widths and penetrability of E_r at the channel radius $a = 5$ fm as often done in structure model calculations. The levels connected by dashed lines are the linear-chain band members. For comparison, theoretical results of the linear-chain bands predicted in two other calculations [34,40]. The theoretical widths are not necessarily consistent between the three calculations, mainly because of different theoretical values of E_r, which are affected by the model ambiguity from effective nuclear interactions and model spaces. However, the dimensionless reduced widths $\theta(a)^2$ are not so much different: $\theta(a)^2$ for the 0^+, 2^+, and 4^+ states are 0.15, 0.27, and 0.10 at $a = 5$ fm in the present calculation, 0.16, 0.15, and 0.09 at $a = 5$ fm in Ref. [34], and 0.07, 0.07, and 0.05 at $a = 6$ fm in

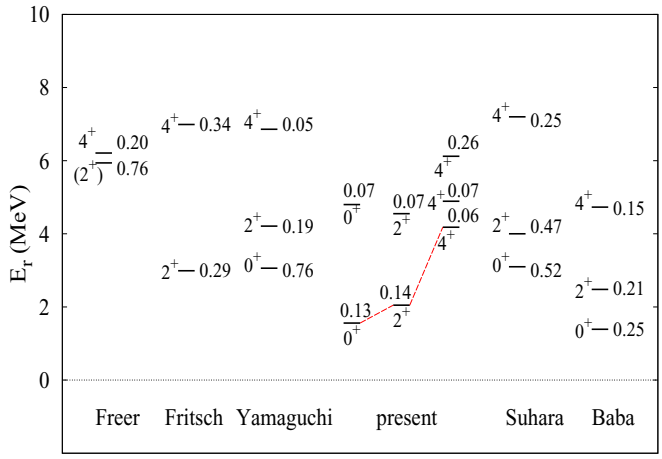

FIG. 4. The calculated energy spectra measured from the ^{10}Be$(0^+_1)+\alpha$ threshold are shown together with ^{10}Be$(0^+_1)+\alpha$ decay widths. The partial decay widths are calculated with the reduced widths and penetrability for α-decay energies (E_r) at the channel radius $a = 5$ fm. The levels connected by dashed lines are the linear-chain band members. In the right two columns, the linear-chain band members predicted in other calculations by Suhara *et al.* [34] and Baba *et al.* [40] are shown. In the left three columns, the 0^+, 2^+, and 4^+ states experimentally observed by α resonant scattering in Ref. [45] by Freer *et al.*, Ref. [46] by Fritsch *et al.*, and Ref. [47] by Yamaguchi *et al.*

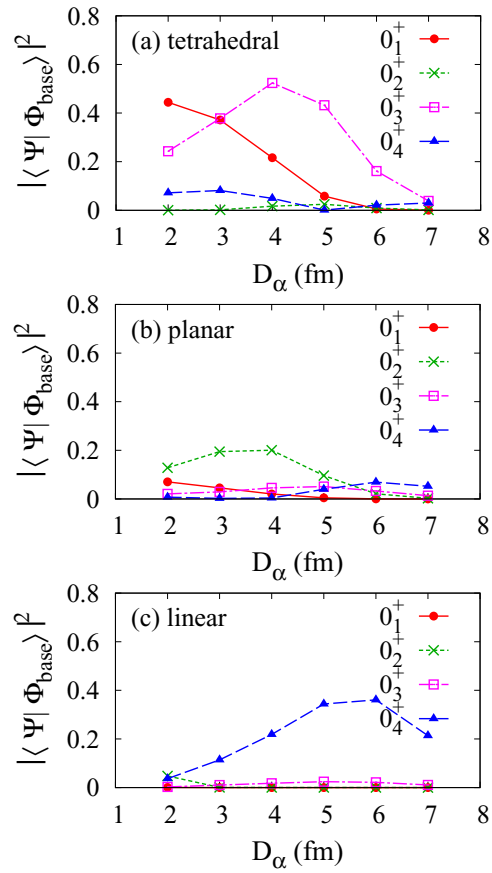

FIG. 5. Components of (a) tetrahedral, (b) planar, and (c) linear configurations contained in 0^+ states. The values of $\mathcal{O}^2_{3\alpha+nn}(d, D_\alpha, \phi, \theta_\alpha)$ given in Eq. (11) with $(\theta_\alpha, \phi) = (\pi/2, 5\pi/8)$, $(\theta_\alpha, \phi) = (\pi/2, \pi/8)$, and $\theta = 0$ for the tetrahedral, planar, and linear configurations, respectively, are plotted as functions of D_α. $d = 4$ fm is chosen for all the configurations.

Ref. [40]. It means that the cluster structure of the linear-chain band is qualitatively similar between these calculations.

The data of 0^+, 2^+, and 4^+ states reported by experiments of the α resonant scattering [45–47] are also shown in left three columns of Fig. 4. It is difficult to confirm the experimental assignment of the linear-chain band from those data because the data are not necessarily consistent between different experiments. The $\theta^2_\alpha(a)$ values at $a = 5$ fm reported in Ref. [47] are 0.34(12), 0.091(27), and 0.024(9) for the 0^+, 2^+, and 4^+ states, respectively. The observed $\theta^2_\alpha(a)$ values of the 2^+ and 4^+ states are smaller than the present result.

C. $3\alpha + nn$ cluster structures

As mentioned previously, the remarkable monopole transition strength is obtained for the 0^+_3 state, whereas the strengths of the 0^+_2 and 0^+_4 states are relatively weak. These features of monopole excitations can be understood by the $3\alpha + nn$ clustering. To clarify properties of the clustering, we calculate the squared overlap $\mathcal{O}^2_{3\alpha+nn}(d, D_\alpha, \phi, \theta_\alpha)$ of $\Psi(J^\pi_k)$ with each $3\alpha + nn$ configuration specified by the parameters D_α, θ_α, and ϕ as given in Eq. (11). D_α and θ_α describe the position of the third α cluster around the ^{10}Be core, and ϕ is the parameter for the *nn* orientation against the 3α plane (see Fig. 1). We categorize $\Phi_{3\alpha+nn}(d, D_\alpha, \phi, \theta_\alpha)$ into three types of wave functions as "tetrahedral," "planar," and "linear" configurations with $(\theta_\alpha, \phi) = (\pi/2, 5\pi/8)$, $(\theta_\alpha, \phi) = (\pi/2, \pi/8)$, and $\theta_\alpha = 0$, respectively. Each component contained in J^π_k states is evaluated with $\mathcal{O}^2_{3\alpha+nn}(d, D_\alpha, \phi, \theta_\alpha)$ for the corresponding configuration. Figure 5 shows components of the tetrahedral, planar, and linear configurations. Obtained values of $\mathcal{O}^2_{3\alpha+nn}(d, D_\alpha, \phi, \theta_\alpha)$ are plotted as functions of the distance D_α of the third α from the subsystem $2\alpha + nn$. Here, we show the result for $d = 4$ fm of the α-α distance in the $2\alpha + nn$ part in order to discuss prominent cluster features. As shown in Fig. 5(a) for the tetrahedral, the ground state contains components of the compact tetrahedral configuration, and the 0^+_3 state can be regarded as a vibration mode of the triangle 3α in the tetrahedral configuration. This excitation mode of the 0^+_3 contributes to the remarkable monopole transition strength because it expresses radial excitation of α clusters keeping the same shape as the 0^+_1 state. The 0^+_4 state contains dominantly the linear component with $D_\alpha = 5$–6 and constructs the linear-chain band with a large momentum of inertia because of the highly elongated shape. The 0^+_2 state shows a weak cluster feature because it is the shell-model state and roughly described by the neutron excitation to the *sd* shell. However, it contains a significant planar component, as can be seen in Fig. 5(a). From this feature found in the mapping onto the cluster model space, one can interpret the 0^+_2 state as the excitation from the compact tetrahedral configuration of the ground state into the planar configuration. Such excitations into the planar and linear configurations obtained in

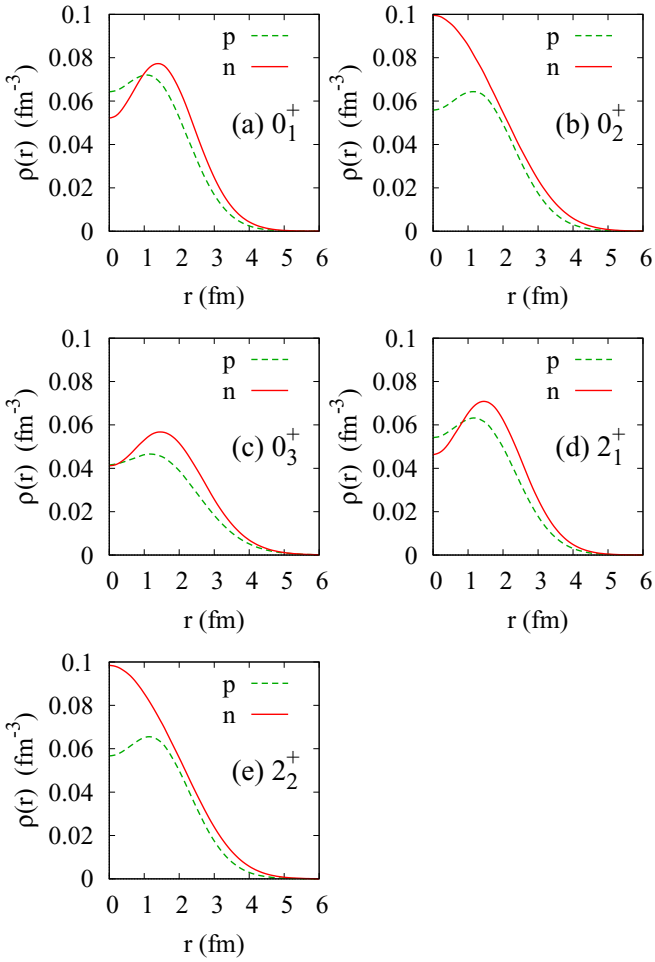

FIG. 6. Proton and neutron densities for (a) 0^+_1, (b) 0^+_2, (c) 0^+_3, (d) 2^+_1, and (e) 2^+_2 of ^{14}C calculated with VAP+cl-GCM.

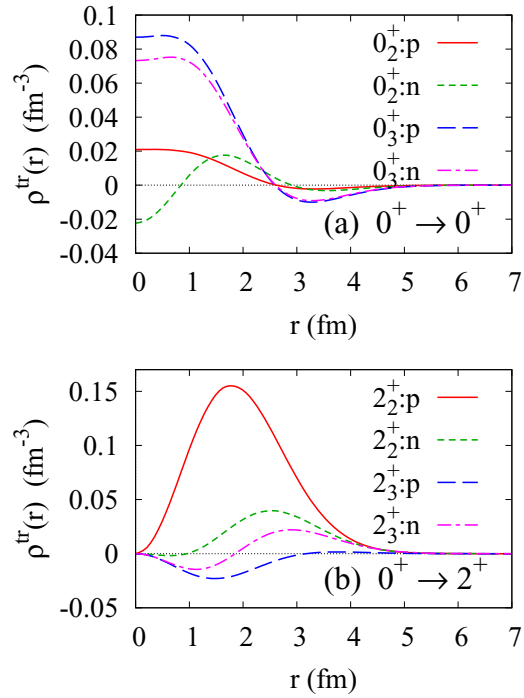

FIG. 7. Proton and neutron transition densities for (a) $0^+_1 \to 0^+_{2,3}$ and (b) $0^+_1 \to 2^+_{1,2}$ of ^{14}C calculated with VAP+cl-GCM.

the 0^+_2 and 0^+_4 states involve drastic changes of the geometric structure from the ground state and describe suppression of monopole transitions in general.

It should be commented that the squared overlap $\mathcal{O}_{3\alpha+nn}(d, D_\alpha, \phi, \theta_\alpha)$ is not concentrated on a specific configuration but somewhat fragmented. It indicates non negligible configuration mixing and also may suggest coupling with continuum states.

In the present calculation of VAP+cl-GCM, the linear-chain band is built on the 0^+_4 state in the $3\alpha + nn$ cluster dynamics. This result is qualitatively similar to that of the previous calculation with the $3\alpha + nn$-cluster model [39]. On the other hand, the AMD calculations in Refs. [34,37,40] obtained the linear-chain state as the 0^+_3 state, which means that a low-lying monopole excitation was missing in the AMD calculations because they do not fully take into account $3\alpha + nn$ cluster configurations.

IV. α INELASTIC SCATTERING OFF ^{14}C

As a probe of cluster states, we investigate the α inelastic scattering off ^{14}C with the MCC calculation. Particular attention is paid to the inelastic scattering of the 0^+_3 having a strong monopole transition, which is expected to be strongly populated by α scattering. For this state, the monopole transition matrix elements $M_p(E0)$ and $M_n(E0)$ of the proton and neutron parts are predicted to be $M_p(E0) = 4.3$ fm^2 and $M_n(E0) = 3.9$ fm^2, which are of the same order as $M_p(E0) = 5.48 \pm 0.22$ fm^2 of ^{12}C(0^+_2) measured by electron pair emission [73].

The α inelastic-scattering cross sections of the 0^+ and 2^+ states of ^{14}C are calculated by using the matter and transition densities obtained by the present VAP+cl-GCM calculation. The calculated proton and neutron densities and transition densities are shown in Figs. 6 and 7, respectively. The reaction calculation is in principle the same approach as that of our previous works on the ^{12}C(α, α') and ^{16}O(α, α'), which successfully reproduced inelastic cross sections of cluster states. The α-nucleus CC potentials are microscopically derived by folding the Melbourne g-matrix effective NN interaction [74] with an α density and the matter and transition densities of ^{14}C. The channel-coupling of $\lambda = 0$ and $\lambda = 2$ transitions for the $0^+_{1,\ldots,10}$ and $2^+_{1,\ldots,10}$ states theoretically obtained by VAP+cl-GCM are taken into account.

The calculated α scattering cross sections of ^{14}C(0^+) at incident energies of $E_\alpha = 140$ and 400 MeV and those of ^{14}C(2^+) states are shown in Figs. 8 and 9, respectively. The strong monopole excitation to the 0^+_3 state by the α scattering is predicted because of the remarkable isoscalar monopole transition. Inelastic cross sections of the 0^+_4 state are relatively small. This is consistent with the weak isoscalar monopole transitions from the ground states in prediction of the structure calculation. Among the 2^+ states, the cross sections of the 2^+_1

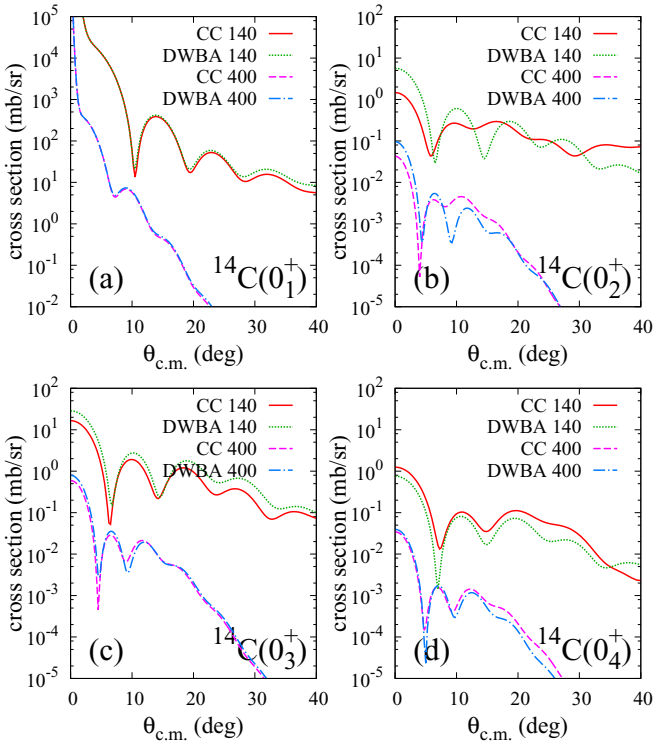

FIG. 8. 0^+ cross sections of the α scattering off ^{14}C obtained with the MCC and distorted wave Born approximation calculations at incident energies of $E_\alpha = 140$ MeV and 400 ($\times 10^{-2}$) MeV.

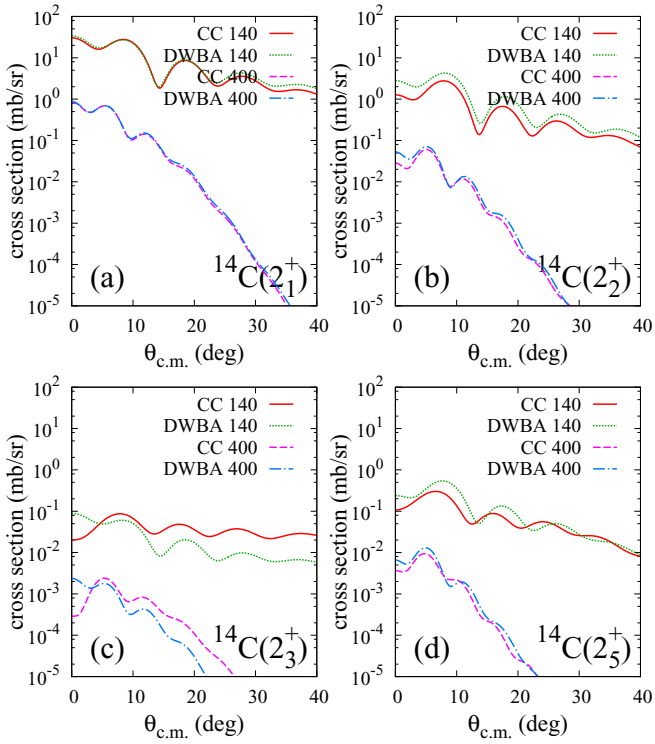

FIG. 9. 2^+ cross sections of the α scattering off ^{14}C obtained with the MCC and distorted wave Born approximation calculations at incident energies of $E_\alpha = 140$ MeV and 400 ($\times 10^{-2}$) MeV.

state in the ground band are significantly large, but those of other 2^+ states are relatively small.

There is no α scattering experiment that observed the 0^+_3 and 0^+_4 states. From the present prediction of the enhanced 0^+_3 cross sections, one expects strong population of the 0^+_3 state in the α scattering. On the other hand, the present result suggests relatively weak productions of the linear-chain states, the 0^+_4 and 2^+_5 states of ^{14}C, even though they have a developed cluster structure. However, as seen in Figs. 8 and 9, the CC effect is minor for the cross sections to those linear-chain states at $E_\alpha = 400$ MeV. This result may suggest a possibility of observing the predicted 0^+_4 and 2^+_5 states in the linear-chain band via a multipole decomposition analysis of differential cross sections of α scattering.

V. SUMMARY

Cluster features of ^{14}C were investigated with VAP+cl-GCM, which is a method of AMD combined with the $3\alpha + nn$ cluster model. In the structure calculation of ^{14}C, the AMD wave functions obtained with the variation after parity and angular-momentum projections for ^{14}C($0^+_{1,2}$), ^{14}C($2^+_{1,2}$), and ^{14}C(1^+_1) are used. In addition to the AMD wave functions, $3\alpha + nn$ wave functions are superposed with GCM to take into account large-amplitude cluster motion.

The energy spectra and band structures of 0^+, 2^+, and 4^+ states were discussed. The 0^+_3 and 0^+_4 states with prominent cluster structures were obtained. The 0^+_3 state has the remarkable monopole transitions from the ground state and is regarded as the vibrational mode of the triangle 3α configuration. The 0^+_4 state contains dominantly the linear-chain 3α structure with two neutrons. The cluster feature of the 0^+_4 state is qualitatively consistent with the 0^+_4 state obtained with the $3\alpha + nn$ cluster model calculation in Ref. [39], and similar to the 0^+_3 state of the AMD predictions in Refs. [34,37,40].

The ^{10}Be(0^+_1) + α components and the α-decay widths were discussed. The calculated result for the linear-chain band was compared with the observed data reported by α resonant scattering experiments [45–47]. Properties for other decay channel such as the ^{10}Be(2^+_1) + α channel were not discussed. For the bandhead state, the ^{10}Be(2^+_1) + α decay may be suppressed because of larger penetrability compared with the ^{10}Be(0^+_1) + α decay for the bandhead 0^+ state but it may contribute to total decay widths of higher spin states.

The α inelastic scattering off ^{14}C at $E_\alpha = 140$ and 400 MeV were also calculated by the MCC calculation with the Melbourne g-matrix interaction for the folding model by utilizing the matter and transition densities obtained from the structure calculation. The calculation predicts enhanced monopole cross sections for the 0^+_3 state because of the remarkable monopole transition strength and suggests a possible observation of the 0^+_3 state via an α inelastic-scattering experiment in the future. For the 0^+_4 and 2^+_5 states of the linear-chain band, the result shows smaller cross sections compared with the 2^+_1 and 0^+_3 states.

In the present calculation, we could not draw a definite assignment of the obtained linear-chain band to observed levels because model ambiguities remain and also experimental information is still limited. In the experimental side, many states have been observed near and above the ^{10}Be $+\alpha$ threshold energy. The α inelastic scattering can be a good probe for the monopole excitation of the triangle vibration mode predicted as the 0_3^+ state. For the linear-chain band, the present calculation predicts relatively weaker production of the 0_4^+ and 2_5^+ states in the α scattering. Nevertheless, the CC effect is minor for the cross sections to those linear-chain states at $E_\alpha = 400$ MeV. This result may suggest a possibility of observing the predicted linear-chain band via a multipole decomposition analysis of differential cross sections of α scattering.

ACKNOWLEDGMENTS

The computational calculations of this work were performed by using the supercomputer in the Yukawa Institute for theoretical physics, Kyoto University. This work was partly supported by Grants-in-Aid of the Japan Society for the Promotion of Science (Grants No. JP18K03617, No. JP16K05352, and No. 18H05407) and by the grant for the RCNP joint research project.

[1] Y. Fujiwara, Y. Suzuki, H. Horiuchi, K. Ikeda, M. Kamimura, K. Katō, Y. Suzuki, and E. Uegaki, Prog. Theor. Phys. Suppl. **68**, 29 (1980).
[2] T. Yamada, Y. Funaki, H. Horiuchi, G. Roepke, P. Schuck, and A. Tohsaki, Lect. Notes Phys. **848**, 229 (2012).
[3] H. Horiuchi, K. Ikeda, and K. Katō, Prog. Theor. Phys. Suppl. **192**, 1 (2012).
[4] M. Freer and H. O. U. Fynbo, Prog. Part. Nucl. Phys. **78**, 1 (2014).
[5] Y. Funaki, H. Horiuchi, and A. Tohsaki, Prog. Part. Nucl. Phys. **82**, 78 (2015).
[6] M. Freer, H. Horiuchi, Y. Kanada-En'yo, D. Lee, and Ulf-G. Meißner, Rev. Mod. Phys. **90**, 035004 (2018).
[7] Y. Fukushima and M. Kamimura, J. Phys. Soc. Jpn. **44**, 225 (1978).
[8] E. Uegaki, S. Okabe, Y. Abe, and H. Tanaka, Prog. Theor. Phys. **57**, 1262 (1977).
[9] E. Uegaki, Y. Abe, S. Okabe, and H. Tanaka, Prog. Theor. Phys. **62**, 1621 (1979).
[10] M. Kamimura, Nucl. Phys. A **351**, 456 (1981).
[11] P. Descouvemont and D. Baye, Phys. Rev. C **36**, 54 (1987).
[12] Y. Kanada-En'yo, Phys. Rev. Lett. **81**, 5291 (1998).
[13] A. Tohsaki, H. Horiuchi, P. Schuck, and G. Ropke, Phys. Rev. Lett. **87**, 192501 (2001).
[14] Y. Funaki, A. Tohsaki, H. Horiuchi, P. Schuck, and G. Ropke, Phys. Rev. C **67**, 051306(R) (2003).
[15] T. Neff and H. Feldmeier, Nucl. Phys. A **738**, 357 (2004).
[16] S. I. Fedotov, O. I. Kartavtsev, V. I. Kochkin, and A. V. Malykh, Phys. Rev. C **70**, 014006 (2004).
[17] C. Kurokawa and K. Katō, Nucl. Phys. A **738**, 455 (2004).
[18] C. Kurokawa and K. Kato, Phys. Rev. C **71**, 021301(R) (2005).
[19] I. Filikhin, V. M. Suslov, and B. Vlahovic, J. Phys. G **31**, 1207 (2005).
[20] Y. Funaki, H. Horiuchi, and A. Tohsaki, Prog. Theor. Phys. **115**, 115 (2006).
[21] Y. Kanada-En'yo, Prog. Theor. Phys. **117**, 655 (2007); **121**, 895 (2009).
[22] K. Arai, Phys. Rev. C **74**, 064311 (2006).
[23] M. Chernykh, H. Feldmeier, T. Neff, P. von Neumann-Cosel, and A. Richter, Phys. Rev. Lett. **98**, 032501 (2007).
[24] S. Ohtsubo, Y. Fukushima, M. Kamimura, and E. Hiyama, Prog. Theor. Exp. Phys. **2013**, 073D02 (2013).
[25] E. Epelbaum, H. Krebs, T. A. Lahde, D. Lee, and Ulf-G. Meißner, Phys. Rev. Lett. **109**, 252501 (2012).
[26] A. C. Dreyfuss, K. D. Launey, T. Dytrych, J. P. Draayer, and C. Bahri, Phys. Lett. B **727**, 511 (2013).
[27] S. Ishikawa, Phys. Rev. C **90**, 061604(R) (2014).
[28] T. Suhara and Y. Kanada-En'yo, Phys. Rev. C **91**, 024315 (2015).
[29] Y. Funaki, Phys. Rev. C **92**, 021302(R) (2015).
[30] H. Morinaga, Phys. Rev. **101**, 254 (1956).
[31] H. Morinaga, Phys. Lett. **21**, 78 (1966).
[32] N. Itagaki, S. Okabe, K. Ikeda, and I. Tanihata, Phys. Rev. C **64**, 014301 (2001).
[33] N. Itagaki, W. von Oertzen, and S. Okabe, Phys. Rev. C **74**, 067304 (2006).
[34] T. Suhara and Y. Kanada-En'yo, Phys. Rev. C **82**, 044301 (2010).
[35] T. Suhara and Y. Kanada-En'yo, Phys. Rev. C **84**, 024328 (2011).
[36] J. A. Maruhn, N. Loebl, N. Itagaki, and M. Kimura, Nucl. Phys. A **833**, 1 (2010).
[37] T. Baba, Y. Chiba, and M. Kimura, Phys. Rev. C **90**, 064319 (2014).
[38] T. Baba and M. Kimura, Phys. Rev. C **94**, 044303 (2016).
[39] Yuta Yoshida and Yoshiko Kanada-En'yo, Prog. Theor. Exp. Phys. **2016**, 123D04 (2016).
[40] T. Baba and M. Kimura, Phys. Rev. C **95**, 064318 (2017).
[41] N. Soic *et al.*, Phys. Rev. C **68**, 014321 (2003).
[42] W. von Oertzen, H. G. Bohlen, M. Milin, Tz. Kokalova, S. Thummerer, A. Tumino, R. Kalpakpakchieva, T. N. Massey, Y. Eisermann, G. Graw, T. Faestermann, R. Hertenberger, and H.-F. Wirth, Eur. Phys. J. A **21**, 193 (2004).
[43] D. L. Price *et al.*, Phys. Rev. C **75**, 014305 (2007).
[44] P. J. Haigh *et al.*, Phys. Rev. C **78**, 014319 (2008).
[45] M. Freer *et al.*, Phys. Rev. C **90**, 054324 (2014).
[46] A. Fritsch *et al.*, Phys. Rev. C **93**, 014321 (2016).
[47] H. Yamaguchi *et al.*, Phys. Lett. B **766**, 11 (2017).
[48] Z. Y. Tian *et al.*, Chin. Phys. C **40**, 111001 (2016).
[49] T. Kawabata, H. Akimune, H. Fujita, Y. Fujita, M. Fujiwara, K. Hara, K. Hatanaka, M. Itoh *et al.*, Phys. Lett. B **646**, 6 (2007).
[50] Y. Kanada-En'yo, Phys. Rev. C **75**, 024302 (2007).
[51] Y. Funaki, A. Tohsaki, H. Horiuchi, P. Schuck, and G. Ropke, Eur. Phys. J. A **28**, 259 (2006).
[52] T. Yamada1, Y. Funaki, H. Horiuchi, K. Ikeda, and A. Tohsaki, Prog. Theor. Phys. **120**, 1139 (2008).
[53] T. Yamada, Y. Funaki, T. Myo, H. Horiuchi, K. Ikeda, G. Ropke, P. Schuck, and A. Tohsaki, Phys. Rev. C **85**, 034315 (2012).

[54] T. Wakasa, E. Ihara, K. Fujita, Y. Funaki, K. Hatanaka, H. Horiuchi, M. Itoh, J. Kamiya *et al.*, Phys. Lett. B **653**, 173 (2007).
[55] M. Itoh *et al.*, Phys. Rev. C **84**, 054308 (2011).
[56] Y. Chiba and M. Kimura, Phys. Rev. C **91**, 061302(R) (2015).
[57] Y. Kanada-En'yo, H. Horiuchi, and A. Ono, Phys. Rev. C **52**, 628 (1995).
[58] Y. Kanada-En'yo and H. Horiuchi, Prog. Theor. Phys. Suppl. **142**, 205 (2001).
[59] Y. Kanada-En'yo, M. Kimura, and A. Ono, Prog. Theor. Exp. Phys. **2012**, 01A202 (2012).
[60] Y. Kanada-En'yo and T. Suhara, Phys. Rev. C **89**, 044313 (2014).
[61] K. Minomo and K. Ogata, Phys. Rev. C **93**, 051601(R) (2016).
[62] Y. Kanada-En'yo and K. Ogata, Phys. Rev. C **99**, 064601 (2019).
[63] Y. Kanada-En'yo and K. Ogata, Phys. Rev. C **99**, 064608 (2019).
[64] N. Itagaki, H. Masui, M. Ito, and S. Aoyama, Phys. Rev. C **71**, 064307 (2005).
[65] D. M. Brink, *Proc. Int. School of Physics Enrico Fermi, Course 36*, Varenna, edited by C. Bloch (Academic Press, New York, 1966).
[66] T. Ando, K. Ikeda, and A. Tohsaki, Prog. Theor. Phys. **64**, 1608 (1980).
[67] R. Tamagaki, Prog. Theor. Phys. **39**, 91 (1968).
[68] N. Yamaguchi, T. Kasahara, S. Nagata, and Y. Akaishi, Prog. Theor. Phys. **62**, 1018 (1979).
[69] A. Volkov, Nucl. Phys. **74**, 33 (1965).
[70] F. Ajzenberg-Selove, Nucl. Phys. A **523**, 1 (1991).
[71] I. Angeli and K. P. Marinova, At. Data Nucl. Data Tables **99**, 69 (2013).
[72] Y. Kanada-En'yo, T. Suhara, and Y. Taniguchi, Prog. Theor. Exp. Phys. **2014**, 073D02 (2014).
[73] J. H. Kelley, J. E. Purcell, and C. G. Sheu, Nucl. Phys. A **968**, 71 (2017).
[74] K. Amos, P. J. Dortmans, H. V. von Geramb, S. Karataglidis, and J. Raynal, Adv. Nucl. Phys. **25**, 275 (2000).